Direct generation of vector vortex beams with switchable radial and azimuthal polarizations in a monolithic Nd:YAG microchip laser

Hong-Sen He, Zhen Chen, and Jun Dong*

Laboratory of Laser and Applied Photonics (LLAP), Department of Electronics Engineering, Xiamen University, Xiamen 361005, China

*E-mail: jdong@xmu.edu.cn

A hollow focus lens (HFL) has been designed to effectively produce a focused annular beam for high-intensity pumping. By applying the central-dark pump beam, a monolithic Nd:YAG microchip laser without any extra optical elements is demonstrated to generate vector vortex beams with switchable radially polarized (RP) and azimuthally polarized (AP) states by easily controlling the pump power. The order and handedness of the output vortex beam remain stable during the switching of the RP and AP states. The monolithic Nd:YAG microchip laser provides a new laser source for applications such as material processing and optical manipulation. © 2017 The Japan Society of Applied Physics

Cylindrical vector (CV) beams are one of the vector-beam solutions of Maxwell's equations. Radially polarized (RP) and azimuthally polarized (AP) beams are distinguished CV beams and have extensive applications in, for example, imaging and sensing, material processing, and optical manipulation.[1] The vortex beam with the spiral wavefront can also be derived from Maxwell's equations and carries orbital angular momentum.[2] In recent years, the generation and application of the vector vortex beam have received much attention owing to its combined properties of spatial polarization modulation and the helical phase, which makes this kind of beam more flexible in beam manipulation than a single vector or vortex beam. The vector vortex beam opens up a variety of new technologies, such as the photonic spin Hall effect,[3] sharper focusing,[4] and laser microprocessing.[5] In most attempts at generating vector vortex beams, extra optical elements such as the q-plate, polarizer, wave plate, spiral phase plate, and digital micro-mirror device are necessary for converting the polarization and phase states of the laser beam outside (passive methods)[6] or inside (active methods)[7,8] the laser cavity. However, in the passive methods, the conversion efficiency and high power operation are limited by the use of those elements. In the active methods, those optical elements not only add intracavity losses but also decrease the damage threshold of the laser, and in particular, the change of the polarization states from the RP mode to the AP mode for the vector vortex beam is complicated and difficult to control. In addition, the long cavity required for inserting extra optical elements makes the laser more intricate.

The key point in exciting vector vortex beams in an end-pumped solid-state laser (EPSSL) is to utilize the annular-shaped beam as the pump source. In recent years, the mode conversion fiber[9] and axicon[10] have been used to produce the annular beam. All of these methods need extra lenses to focus the generated annular beam for high-intensity pumping, and the position of the lens relative to the optical element should be adjusted carefully to produce a good focused annular pump spot; all these findings add to the adjustment complexity. Furthermore, the high costs of the optical elements such as the axicon also hinder the application of vector vortex lasers. Therefore, a low-cost single optical element capable of directly generating focused annular beams is urgently needed.

In this letter, a hollow focus lens has been designed to produce the focused annular beam. By applying the focused
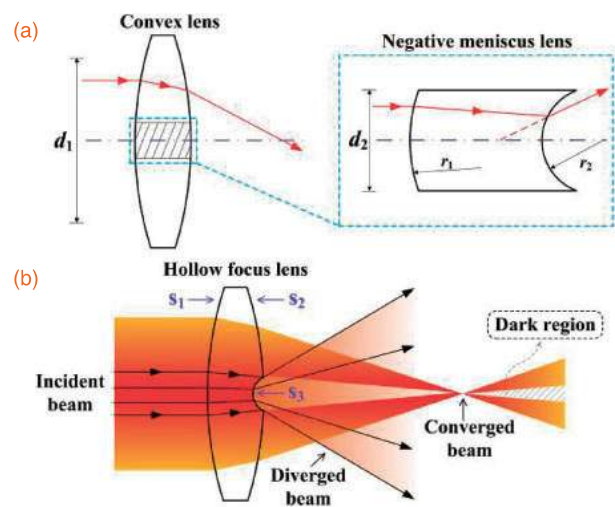

Fig. 1. (a) Principle of the HFL. (b) Optical path of the HFL for generating the focused annular beam.

central-dark pump beam, a monolithic Nd:YAG microchip laser for directly generating vector vortex beams with switchable radially and azimuthally polarized states has been demonstrated. The order and handedness of the output vortex beam remained stable during the switching from the RP state to the AP state. The vector vortex beam was self-sustained in the laser cavity without the use of any mode-selecting elements. The output power of 1.16 W was obtained at the incident pump power of 10 W.

As shown in Fig. 1(a), the hollow focus lens (HFL) is formed by replacing the central region of a convex lens (CL) with a negative meniscus lens (NML). d_1 is the clear aperture of the CL and d_2 is the diameter of the NML. r_1 and r_2 are the curvature radii for the two surfaces of the spherical NML, respectively. r_1 is much larger than r_2 in order to form a negative lens. Figure 1(b) gives the optical path of the HFL for generating the focused annular beam. S_1, S_2, and S_3 denote the back, front, and concave surfaces of the HFL, respectively. When a collimated laser beam is incident on S_1, the output beam is divided into the converged beam from S_1 to S_2 and the diverged beam from S_1 to S_3. The power intensity of the diverged beam can be neglected compared with the converged beam after the lens focal plane when applying appropriate parameters of S_3 and the relative sizes of d_1 and d_2. Therefore, a dark central region exists in the converged beam after the lens focal point, as shown in Fig. 1(b).
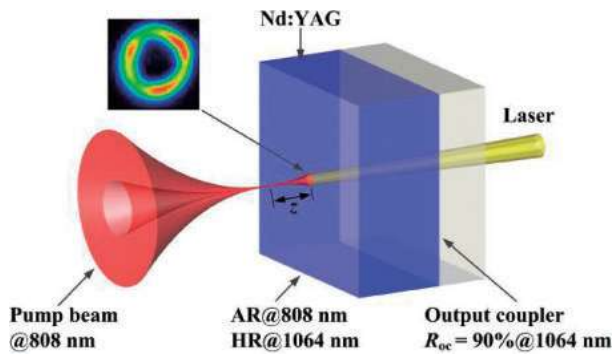
Fig. 2. Schematic diagram of the monolithic Nd:YAG microchip laser for generating the vector vortex beam with switchable RP and AP states.

The schematic diagram of the monolithic Nd:YAG microchip laser for generating the vector vortex beam with switchable RP and AP states is shown in Fig. 2. A 1-mm-thick surface-coated Nd:YAG crystal and a plane–parallel output coupler (OC) were attached closely together by clamps to form the monolithic microchip laser cavity. The doping concentration of Nd^{3+} ions in the Nd:YAG crystal was 1 at. %. The antireflection (AR) coating at 808 nm and the high-reflection (HR) coating at 1064 nm on one surface of the Nd:YAG crystal served as the rear mirror of the resonator. The reflection of the OC (R_{oc}) was 90% at 1064 nm. The pump source was an 808 nm fiber-coupled laser diode. The pump beam was focused by the HFL with the focal length of 8 mm. The rear mirror of the resonator was placed away from the lens focal point at a distance of $z = 0.2$ mm such that the incident pump beam on the Nd:YAG crystal was annular with a dark central region. The measured intensity distribution of the incident pump beam on the rear mirror of the resonator is shown in the inset of Fig. 2. The diameter of the annular pump beam was measured to be 170 µm. The measured power conversion efficiency when utilizing the HFL to achieve the annular beam was 85.5%, which was much higher than 75% in the method of using the mode conversion fiber.[9] A power meter (Thorlabs PM100D) was used to measure the output laser power. The beam profiles were monitored and recorded using a CCD analyzer (Thorlabs BC106-VIS).

Figure 3(a) shows the intensity distribution of the output laser transverse profile at different incident pump powers (P_{in}). The lasing threshold was 0.7 W. The laser transverse profiles retained their annular shapes with increasing P_{in}. The pump-power-independent annular transverse mode is attributed to the focused pump beam with uniform annular shapes formed by the HFL, which has advantages over the pump-power-dependent transverse laser modes when using the mode conversion fiber.[9] The polarization states of the laser transverse modes were examined using a linear polarizer. It was found that the output laser is in the RP state when $P_{in} < 5.5$ W, which changes to the AP state when $P_{in} > 5.5$ W. Figures 3(b) and 3(c) show the intensity distribution and the examined polarization state of the laser beam at $P_{in} = 5$ and 6 W, respectively. "N" denotes the measured laser transverse profile without the polarizer and the white arrows denote the trans-axis of the polarizer. At $P_{in} = 5$ W, the intensity distributions of the two symmetric lobes were parallel to the trans-axis of the polarizer, proving that the annular laser beam was radially polarized. At $P_{in} = 6$ W, the
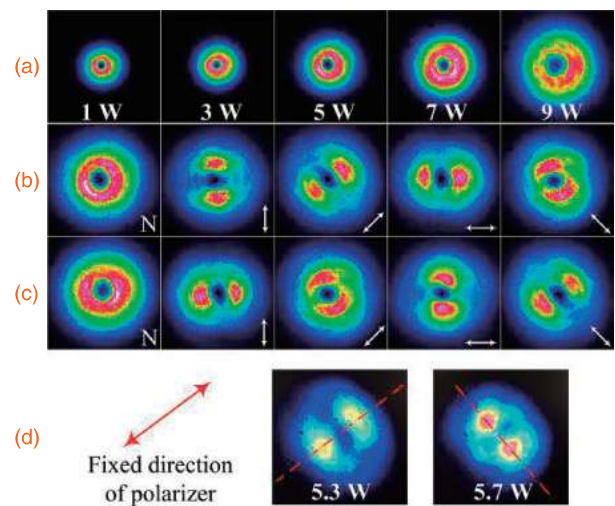

Fig. 3. (a) Intensity distribution of the output laser transverse profile at $P_{in} = 1, 3, 5, 7,$ and 9 W. (b, c) Intensity distribution and examined beam polarization state at $P_{in} = 5$ and 6 W, respectively. (d) Switching from the RP state to the AP state of the laser beam with increasing pump power at a fixed direction of polarizer (see Visualization 1 in the online supplementary data at http://stacks.iop.org/APEX/10/052701/mmedia).
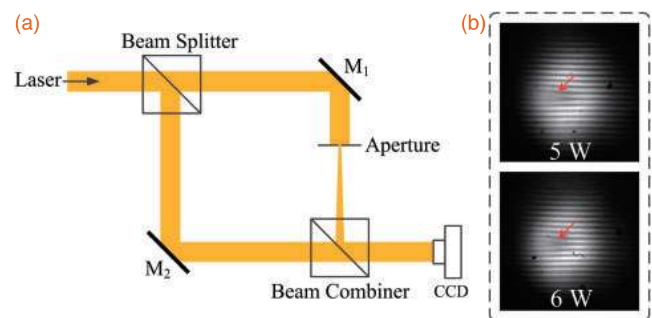

Fig. 4. (a) Mach–Zehnder interferometer for testing the phase structure of the output laser beam. (b) Optical vortex states of the output laser beam at $P_{in} = 5$ and 6 W.

intensity distributions of the two symmetric lobes were perpendicular to the trans-axis of the polarizer, proving that the annular laser beam was azimuthally polarized. Furthermore, the polarization states of the output laser were monitored using the CCD analyzer when P_{in} was increased from 5 to 6 W while the direction of the polarizer was fixed at a certain position. As shown in Fig. 3(d), the two symmetric lobes of the laser beam were parallel to the trans-axis of the polarizer at $P_{in} = 5.3$ W, as denoted by the red lines. Then, the two symmetric lobes were switched to the perpendicular direction when P_{in} was increased to 5.7 W. The switching of the two polarization states of the CV beam occurred at $P_{in} = 5.5$ W, as shown in Visualization 1. Obviously, the CV modes of the output beam can be easily controlled by varying the pump power; this has advantages over adjusting the complex laser cavity to control the CV modes of the output beam in EPSSLs.[11,12]

Figure 4(a) shows the experimental setup of a Mach–Zehnder interferometer for testing the phase structure of the output laser beam. The laser beam was separated into two parts by a beam splitter. M_1 and M_2 were two mirrors for reflecting the laser beam. A tiny aperture was used to select the laser beam in the upper arm to obtain a plane wave to act
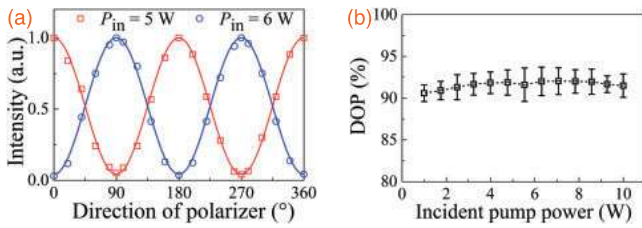
Fig. 5. (a) Laser power intensity of the selected parts of the output laser beam as a function of the polarizer direction at $P_{in} = 5$ and 6 W. (b) DOP of the output laser as a function of P_{in}.

as the probe wave. The laser beams in the two arms were merged together in the beam combiner and then the interference fringes were observed using a CCD analyzer. Figure 4(b) shows the interference fringes of the output laser beam at $P_{in} = 5$ and 6 W. At both $P_{in} = 5$ and 6 W, a forklike fringe exists in the interferogram, as pointed by the red arrow. A single fringe splits into two fringes, which verifies that the output laser possesses a phase singularity at the fork dislocation and the emitting laser is an optical vortex beam of topological charge $l = 1$. In addition, the same split directions of the forklike fringes at the two pump levels imply that the handedness of the helical wavefronts is the same at $P_{in} = 5$ and 6 W. Evidently, the order and handedness of the output vortex beam remain unchanged during the switch from the RP state to the AP state. The stabilization of the optical vortex is attributed to the nearly invariable intracavity losses in the monolithic laser resonator. Because there are no extra intracavity optical elements that act as mode-selecting or loss-controlling elements in the compact laser cavity, the intracavity loss is constant and the single-handedness vortex mode oscillates stably; thus, the handedness of the output vortex beam remains unchanged with changing incident pump power. The vector vortex beam with steady vortex states and switchable CV modes contributes to more flexible and accurate applications in optical manipulation.

The degree of polarization (DOP) of the whole CV laser beam can be represented by that of any point of the annular profile of the output beam, owing to the fact that the local laser beam is linearly polarized for a pure CV beam. Therefore, a tiny aperture was placed behind the laser cavity at a distance of 3 m along the laser path in order to select a small part of the output beam, then a linear polarizer was used to measure the power intensity of the selected laser beam. Figure 5(a) shows the laser power intensity of the selected beam as a function of the polarizer direction at $P_{in} = 5$ and 6 W. Thus, according to the Malus law, the good fit of the squares of the cosine and sine functions with the measured power intensity supports the fact that the output laser beam is radially polarized at $P_{in} = 5$ W and azimuthally polarized at 6 W. The expression of the DOP is $(P_{max} - P_{min})/(P_{max} + P_{min})$, where P_{max} and P_{min} are the top and bottom values of the fitted curves, respectively. Figure 5(b) shows the DOP of the output laser as a function of P_{in}. The DOP increases from 90.6 to 91.9% when P_{in} increases from 1 to 4.8 W and then exhibits a slight decline of 0.3% at $P_{in} = 5.5$ W. With further increase in P_{in}, the DOP shows a mild fluctuation from 92.1 to 91.4%. Obviously, the DOP remains at around 91% with increasing pump power, and the switch of the RP state to the AP states has a slight influence

on the stabilization of the DOP, making the monolithic Nd:YAG microchip laser more suitable for practical applications.

The self-sustained oscillation of the RP and AP laser modes in the annular-beam-pumped microchip laser is caused by the thermal-lens-effect-induced bifocusing effect in the Nd:YAG crystal.[13] The transition from the RP laser mode to the AP laser mode in the Nd:YAG microchip laser is attributed to the localized oscillating laser (LOL) spot size and the overlap efficiencies between the LOL spot size and the localized pump region (LPR) spot size for the P_r-polarized and P_ϕ-polarized laser modes. The annular pump region can be divided into infinitely tiny portions that can each be assumed to be an LPR with a Gaussian pump profile.[10] Because of the inhomogeneous intensity distribution of the Gaussian pump beam, the thermally induced optical path difference inside the Nd:YAG crystal creates a thin thermal lens near the rear mirror of the laser cavity. The LOL spot size is determined by the corresponding LPR and the polarization directions of the LOL along the radial and azimuthal directions of the hollow pump region, where the two directions are denoted as P_r and P_ϕ, respectively. The overlap efficiency in the EPSSL is expressed as the ratio of the LPR spot size to the LOL spot size on the cavity rear mirror.[14] The LOL spot sizes of the P_r-polarized and P_ϕ-polarized laser modes strongly depend on the thermal focal length governed by the pump power. The thermal focal length for the P_r-polarized and P_ϕ-polarized LOL modes[15] is given by

$$f_i = \frac{2K\pi r_0^2}{P_{in}\eta} \left[\frac{dn}{dT} - \frac{n_0^3 \alpha C_i}{48(1-\nu)} + \frac{2(n_0 - 1)\alpha l_0}{L} \right]^{-1},$$
$$i = r, \phi, \quad (1)$$

where K is the thermal conductivity, r_0 is the LOL spot radius, L is the crystal length, η is the effective fraction of pump power converted to heat, n_0 is the crystal refractive index, ν is the Poisson ratio, α is the thermal expansion coefficient, and l_0 is the expansion length of the crystal. The parameters of the Nd:YAG crystal used in the calculation are taken from Ref. 15. C_i is the photoelastic coefficient, which is only affected by the inner structure of the Nd:YAG crystal.[16] r denotes the P_r-polarized LOL and ϕ denotes the P_ϕ-polarized LOL ($C_r = -1.311$ and $C_\phi = 0.17$[15]). The spot size of the LOL mode on the rear mirror of the laser cavity[17] can be expressed as

$$\omega_i^2 = \frac{\lambda L}{\pi n_0} \sqrt{\frac{g_2}{g_{1i}(1 - g_{1i}g_2)}}, \quad i = r, \phi, \quad (2)$$

where $g_{1i} = 1 - n_0 L/(2f_i)$, $g_2 = 1$, and λ is the laser wavelength at 1064 nm.

Figure 6 shows the LOL spot size and the overlap efficiencies with the LPR spot size for the P_r-polarized and P_ϕ-polarized laser modes as a function of P_{in}. For the same P_{in}, the P_r-polarized laser mode spot size is smaller than the P_ϕ-polarized laser mode spot size when $P_{in} < 5.5$ W. The P_r-polarized laser mode spot size becomes larger with further increase in P_{in}. The calculated LOL spot size is larger than the measured spot size (19 μm) of the LPR owing to the gain guiding effect.[18] Thus, a larger laser spot size degrades the overlap efficiency with the pump beam. As shown in Fig. 6, for the same P_{in}, the overlap efficiency for the P_r-polarized laser mode is greater than that for the P_ϕ-polarized laser mode
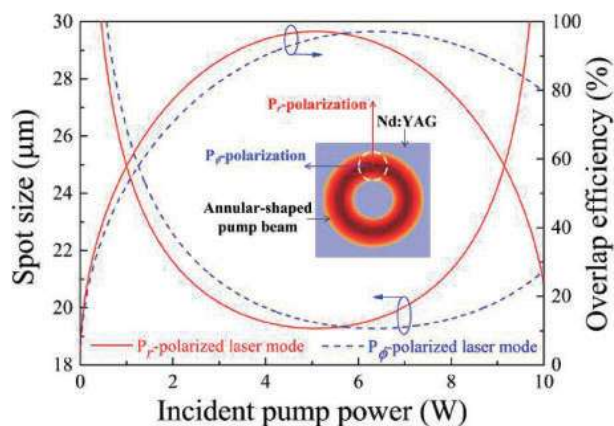
Fig. 6. LOL spot size and the corresponding overlap efficiencies with the LPR spot size for P_r-polarized and P_ϕ-polarized laser modes as a function of P_{in}. Inset: the cross section of the annular pump beam incident on the surface of the Nd:YAG crystal. The white dashed circle denotes one of the divided infinitely tiny portions that serve as an LPR.

when $P_{in} < 5.5$ W, whereas the overlap efficiency for the P_ϕ-polarized laser mode exceeds that for the P_r-polarized laser mode when $P_{in} > 5.5$ W. The higher overlap efficiency between the LPR and the LOL spot size contributes to a lower lasing threshold and a stronger competition for the inversion population inside the Nd:YAG crystal.[19] Therefore, the P_r-polarized LOL mode starts to oscillate first and fully extracts the energy stored in the gain medium, whereas lasing in the P_ϕ-polarized LOL mode is suppressed when $P_{in} < 5.5$ W. With further increase in P_{in}, the overlap efficiency for the P_r-polarized mode is smaller, thus the P_ϕ-polarized laser mode oscillates preferably. Therefore, there is a mode transition from the RP laser mode to the AP laser mode at $P_{in} = 5.5$ W.

The output power was measured by increasing P_{in}. The slope efficiency was 16.8% when $P_{in} < 6.5$ W. The highest output power of 1.16 W was achieved at $P_{in} = 10$ W. The beam propagation factor (M^2) of the output laser was

measured to be <2.6 by increasing pump power, which is in good agreement with the theoretically calculated value of 2 for an ideal first-order Laguerre–Gaussian mode.

In conclusion, a hollow focus lens was designed to form a focused annular pump beam. A vector vortex beam switchable between radial and azimuthal polarizations was generated in a monolithic Nd:YAG microchip laser. The transition from the RP mode to the AP laser mode was attributed to the thermal-lens-dependent localized oscillating laser spot size. The monolithic Nd:YAG microchip laser provides a new method for developing high-power vector vortex beams for practical applications.

1) Q. Zhan, Adv. Opt. Photonics **1**, 1 (2009).
2) L. Allen, M. W. Beijersbergen, R. J. C. Spreeuw, and J. P. Woerdman, Phys. Rev. A **45**, 8185 (1992).
3) Y. Zhang, P. Li, S. Liu, and J. Zhao, Opt. Lett. **40**, 4444 (2015).
4) X. Hao, C. Kuang, T. Wang, and X. Liu, Opt. Lett. **35**, 3928 (2010).
5) O. J. Allegre, W. Perrie, S. P. Edwardson, G. Dearden, and K. G. Watkins, J. Opt. **14**, 085601 (2012).
6) Z. Liu, Y. Liu, Y. Ke, Y. Liu, W. Shu, H. Luo, and S. Wen, Photonics Res. **5**, 15 (2017).
7) D. Naidoo, F. S. Roux, A. Dudley, I. Litvin, B. Piccirillo, L. Marrucci, and A. Forbes, Nat. Photonics **10**, 327 (2016).
8) J. Hamazaki, A. Kawamoto, R. Morita, and T. Omatsu, Opt. Express **16**, 10762 (2008).
9) Z. Fang, K. Xia, Y. Yao, and J. Li, Appl. Phys. B **117**, 219 (2014).
10) M. D. Wei, Y. S. Lai, and K. C. Chang, Opt. Lett. **38**, 2443 (2013).
11) K. C. Chang, T. Lin, and M. D. Wei, Opt. Express **21**, 16035 (2013).
12) I. Moshe, S. Jackel, and A. Meir, Opt. Lett. **28**, 807 (2003).
13) G. Machavariani, Y. Lumer, I. Moshe, A. Meir, S. Jackel, and N. Davidson, Appl. Opt. **46**, 3304 (2007).
14) C. Y. Li and J. Dong, J. Mod. Opt. **63**, 1323 (2016).
15) W. Koechner, Appl. Opt. **9**, 2548 (1970).
16) J. Foster and L. Osterink, J. Appl. Phys. **41**, 3656 (1970).
17) R. Hauck, H. P. Kortz, and H. Weber, Appl. Opt. **19**, 598 (1980).
18) F. Salin and J. Squier, Opt. Lett. **17**, 1352 (1992).
19) H. S. He, M. M. Zhang, J. Dong, and K. I. Ueda, J. Opt. **18**, 125202 (2016).